Q-anisotropy in finely-layered media

Stefano Picotti,[1] José M. Carcione,[1] Juan E. Santos,[2,3] and Davide Gei[1]

Received 5 December 2009; revised 15 January 2010; accepted 26 January 2010; published 19 March 2010.

[1] Finely layered media behaves as an anisotropic medium at long wavelengths. If the constituent media are anelastic, *Q*-anisotropy of qP, qSV and SH waves can be described by a generalization of Backus averaging to the lossy case. To test the theory, we introduce a novel method to obtain the complex and frequency-dependent stiffnesses from numerical simulations of oscillatory (harmonic) tests based on a space-frequency domain finite element method. We apply the methodology to a periodic sequence of shale and limestone and compute the quality factor and wave velocities as a function of frequency and propagation direction. **Citation:** Picotti, S., J. M. Carcione, J. E. Santos, and D. Gei (2010), *Q*-anisotropy in finely-layered media, *Geophys. Res. Lett.*, *37*, L06302, doi:10.1029/2009GL042046.

1. Introduction

[2] Recent advances in seismic exploration are aimed on property estimates of target zones using amplitude versus offset (AVO) analysis. The broad field of applications reaches from ocean-bottom cable recordings over reservoir permeability estimates to carbon-dioxide sequestration and monitoring. These approaches are heavily affected by the presence of attenuation anisotropy. This has a significant impact on AVO analysis [e.g., *Carcione et al.*, 1998b]. The physical reasons for wave attenuation and attenuation anisotropy are still not completely known. Interlayering could be a major agent beside porosity effects.

[3] Most geological systems can be modeled as fine layering, which refers to the case where the dominant wavelength of the pulse is much larger than the thicknesses of the single layers. When this occurs, the medium is effectively anisotropic with a transversely isotropic symmetry. The first to obtain a solution to this problem was *Bruggeman* [1937]. Other investigators studied the problem using different approaches, e.g., *Riznichenko* [1949] and *Postma* [1955], who considered a two-constituent periodically layered medium. Later, *Backus* [1962] obtained the average elasticity constants in the case when the single layers are transversely isotropic with the symmetry axis perpendicular to the layering plane. Moreover, he assumed stationarity, i.e., in a given length of composite medium much smaller than the wavelength, the proportion of each material is constant (periodicity is not required). The equations were further generalized by *Schoenberg and Muir* [1989] for anisotropic single constituents. Backus averaging for the lossless case has been verified numerically by *Carcione et al.* [1991]. They found that the minimum ratio between the P-wave dominant pulse wavelength and the spatial period of the layering depends on the contrast between the constituents. For instance, for a periodic sequence of epoxy-glass it is around 8, and for sandstone-limestone (which has a lower reflection coefficient) it is between 5 and 6. In any case, an optimal ratio can be found for which the equivalence between a finely layered medium and a homogeneous transversely isotropic medium is valid. *Carcione* [1992] generalized Backus averaging to the anelastic case, obtaining the first model for *Q*-anisotropy [see *Carcione*, 2007]. Analyses on sequences of sandstone-limestone and shale-limestone with different degrees of anisotropy indicate that the quality factors of the shear modes are more anisotropic than the corresponding phase velocities, cusps of the qSV mode are more pronounced for low frequencies and midrange proportions, and in general, attenuation is higher in the direction perpendicular to layering or close to it, provided that the material with lower velocity is the more dissipative. Other alternative models of *Q*-anisotropy were proposed by *Carcione and Cavallini* [1994, 1995] and *Carcione et al.* [1998a]. A brief description of all these models can be found from *Carcione* [2007].

[4] In order to test Backus averaging for *Q*-anisotropy, we perform numerical simulations using an upscaling procedure to obtain the complex stiffnesses of the effective viscoelastic transversely isotropic medium. It consists in the simulation of oscillatory compressibility and shear tests in the space-frequency domain, which enable us to obtain the complex stiffnesses. The method is illustrated by *Santos et al.* [2009] for isotropic media and it is generalized here for anisotropic media. We use a finite element method at a single frequency to approximate the solutions of the associated boundary value problems. We obtain the quality factors and velocities as a function of frequency and propagation angle from the complex stiffnesses.

2. Backus Averaging

[5] Fine layering on a scale much finer than the dominant wavelength of the signal yields effective anisotropy, whose elasticity constants are given by Backus averaging [*Backus*, 1962]. *Carcione* [1992] uses this approach and the correspondence principle to study the anisotropic characteristics of attenuation in viscoelastic finely layered media [e.g., *Carcione*, 2007]. Here, we consider that each medium is isotropic and anelastic with complex Lamé constants given by

$$\lambda(\omega) = \rho\left(c_P^2 - \frac{4}{3}c_S^2\right)M_1(\omega) - \frac{2}{3}\rho c_S^2 M_2(\omega) \quad \text{and} \quad \mu(\omega) = \rho c_S^2 M_2(\omega), \tag{1}$$

[1]Istituto Nazionale di Oceanografia e di Geofisica Sperimentale, OGS, Sgonico, Italy.
[2]CONICET, Departamento de Geofísica Aplicada, Facultad Ciencias Astronómicas y Geofísicas, UNLP, La Plata, Argentina.
[3]Also at Purdue University, Department of Mathematics, West Lafayette, IN 47907, USA.

0094-8276/10/2009GL042046

where ω is the angular frequency, M_1 and M_2 are the dilatational and shear complex moduli, respectively, c_P and c_S are the elastic high-frequency limit compressional- and shear wave velocities, and ρ is the density. (in *Carcione* [1992], the relaxed moduli correspond to the elastic limit.)

[6] Omitting the angular-frequency (ω) dependency for brevity, the dilatational modulus is

$$k = \lambda + \frac{2}{3}\mu = \rho\left(c_P^2 - \frac{4}{3}c_S^2\right)M_1, \tag{2}$$

and the P-wave modulus is given by

$$E = k + \frac{4}{3}\mu. \tag{3}$$

[7] According to *Carcione* [1992], the equivalent viscoelastic transversely isotropic medium is defined by the following complex stiffnesses:

$$\begin{aligned} p_{11} &= \langle E - \lambda^2 E^{-1}\rangle + \langle E^{-1}\rangle^{-1}\langle E^{-1}\lambda\rangle^2, \\ p_{33} &= \langle E^{-1}\rangle^{-1}, \\ p_{13} &= \langle E^{-1}\rangle^{-1}\langle E^{-1}\lambda\rangle, \\ p_{55} &= \langle \mu^{-1}\rangle^{-1}, \\ p_{66} &= \langle \mu\rangle, \end{aligned} \tag{4}$$

where $\langle\cdot\rangle$ denotes the thickness weighted average. In the case of a periodic sequence of two alternating layers, equations (4) are similar to those of *Postma* [1955], who considered lossless layers.

[8] The method is valid for any complex modulus describing the anelastic properties of the medium. Here we assume constant quality factors over the frequency range of interest (until about 100 Hz). Such behavior is modelled by a continuous distribution of relaxation mechanisms based on the standard linear solid [*Liu et al.*, 1976; *Ben-Menahem and Singh*, 1981, p. 909]. The dimensionless dilatational and shear complex moduli for a specific frequency can be expressed as

$$M_\nu(\omega) = \left(1 + \frac{2}{\pi Q_{0\nu}}\ln\frac{1 + i\omega\tau_2}{1 + i\omega\tau_1}\right)^{-1}, \tag{5}$$

where τ_1 and τ_2 are time constants, with $\tau_2 < \tau_1$, and $Q_{0\nu}$ defines the value of the quality factor which remains nearly constant over the selected frequency range. The dilatational, S-wave and P-wave quality factors of each single isotropic layer are respectively given by

$$Q_1 = \frac{\mathrm{Re}(k)}{\mathrm{Im}(k)}, \quad Q_S = Q_2 = \frac{\mathrm{Re}(\mu)}{\mathrm{Im}(\mu)}, \quad \text{and} \quad Q_P = \frac{\mathrm{Re}(E)}{\mathrm{Im}(E)}. \tag{6}$$

[9] We consider homogeneous viscoelastic waves [e.g., *Carcione*, 2007]. The complex velocities are the key quantities to obtain the wave velocities and quality factors of the equivalent anisotropic medium. They are given by

$$\begin{aligned} v_{\mathrm{qP}} &= (2\rho)^{-1/2}\sqrt{p_{11}l_1^2 + p_{33}l_3^2 + p_{55} + A}, \\ v_{\mathrm{qSV}} &= (2\rho)^{-1/2}\sqrt{p_{11}l_1^2 + p_{33}l_3^2 + p_{55} - A}, \\ v_{\mathrm{SH}} &= \rho^{-1/2}\sqrt{p_{66}l_1^2 + p_{55}l_3^2}, \\ A &= \sqrt{[(p_{11} - p_{55})l_1^2 + (p_{55} - p_{33})l_3^2]^2 + 4[(p_{13} + p_{55})l_1 l_3]^2}, \end{aligned} \tag{7}$$

[*Auld*, 1990; *Carcione*, 2007, equation (1.79)], where $l_1 = \sin\theta$ and $l_3 = \cos\theta$ are the directions cosines, θ is the propagation angle between the wave number vector and the symmetry axis, and the three velocities correspond to the qP, qS and SH waves, respectively. The modulus of the phase velocity vector is given by

$$v_p = \left[\mathrm{Re}\left(\frac{1}{v}\right)\right]^{-1}, \tag{8}$$

where v represents either v_{qP}, v_{qSV} or v_{SH}. The energy-velocity vector of the qP and qSV waves is given by

$$\frac{\boldsymbol{v}_e}{v_p} = (l_1 + l_3\cot\psi)^{-1}\widehat{\boldsymbol{e}}_1 + (l_1\tan\psi + l_3)^{-1}\widehat{\boldsymbol{e}}_3 \tag{9}$$

[*Carcione*, 2007, equation (6.158)], where

$$\tan\psi = \frac{\mathrm{Re}(\beta^* X + \xi^* W)}{\mathrm{Re}(\beta^* W + \xi^* Z)} \tag{10}$$

defines the angle between the energy-velocity vector and the z-axis, and

$$\begin{aligned} \beta &= \mathrm{pv}\sqrt{A \pm B}, \\ \xi &= \pm\mathrm{pv}\sqrt{A \mp B}, \\ B &= p_{11}l_1^2 - p_{33}l_3^2 + p_{55}\cos 2\theta, \end{aligned} \tag{11}$$

where the asterisk indicates complex conjugate and the upper and lower signs correspond to the qP and qSV waves, respectively. Moreover,

$$\begin{aligned} W &= p_{55}(\xi l_1 + \beta l_3), \\ X &= \beta p_{11}l_1 + \xi p_{13}l_3, \\ Z &= \beta p_{13}l_1 + \xi p_{33}l_3 \end{aligned} \tag{12}$$

[*Carcione*, 2007, equation (6.121)–(6.123)], where "pv" denotes the principal value, which has to be chosen according to established criteria [e.g., *Sidler et al.*, 2008].

[10] On the other hand, the energy velocity of the SH wave is

$$\boldsymbol{v}_e = \frac{v_p}{\rho\mathrm{Re}(v)}\left[l_1\mathrm{Re}\left(\frac{p_{66}}{v}\right)\widehat{\boldsymbol{e}}_1 + l_3\mathrm{Re}\left(\frac{p_{55}}{v}\right)\widehat{\boldsymbol{e}}_3\right] \tag{13}$$

and

$$\tan\psi = \frac{\mathrm{Re}(p_{66}/v)}{\mathrm{Re}(p_{55}/v)}\tan\theta \tag{14}$$

[*Carcione*, 2007, equation (4.115)]. In general, the phase velocity is related to the energy velocity by

$$v_p = v_e\cos(\psi - \theta), \tag{15}$$

where $v_e = |\boldsymbol{v}_e|$. The quality factor is given by

$$Q = \frac{\mathrm{Re}(v^2)}{\mathrm{Im}(v^2)}. \tag{16}$$

[11] The values of the qP quality factor along the layering plane and symmetry axis are

$$Q_{qP}(\theta = \pi/2) = \frac{\mathrm{Re}(p_{11})}{\mathrm{Im}(p_{11})} \quad \text{and} \quad Q_{qP}(\theta = 0) = \frac{\mathrm{Re}(p_{33})}{\mathrm{Im}(p_{33})}, \tag{17}$$

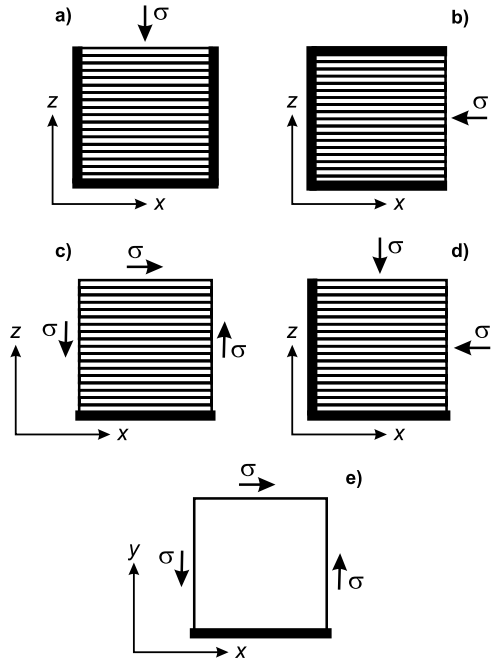

Figure 1. Oscillatory tests performed to obtain (a) p_{33}, (b) p_{11}, (c) p_{55}, (d) p_{13} and (e) p_{66}. The orientation of the layers and the directions of the applied stresses are indicated. The thick black lines at the edges indicate rigid boundary conditions, as defined by equations (24), (25), (27) and (30).

respectively, while those of the shear waves are

$$Q_{qSV}(\theta=\pi/2)=Q_{qSV}(\theta=0)=Q_{SH}(\theta=0)=\frac{\mathrm{Re}(p_{55})}{\mathrm{Im}(p_{55})},\quad \text{and}$$

$$Q_{SH}(\theta=\pi/2)=\frac{\mathrm{Re}(p_{66})}{\mathrm{Im}(p_{66})}. \tag{18}$$

3. Methodology

[12] Let $\boldsymbol{u}$, $\epsilon_{ij}(\boldsymbol{u})$ and $\sigma_{ij}(\boldsymbol{u})$ denote the displacement vector, strain components and stress components of each single medium in the frequency domain. The stress-strain relations are

$$\sigma_{ij}=\lambda\vartheta\delta_{ij}+2\mu\epsilon_{ij},\qquad \vartheta=\epsilon_{ii}=u_{i,i}, \tag{19}$$

where implicit summation of repeated indices is assumed. The equation of motion is

$$\omega^2\rho\boldsymbol{u}(x,z,\omega)+\nabla\cdot\boldsymbol{\sigma}\,[\boldsymbol{u}(x,z,\omega)]=0, \tag{20}$$

where the dot denotes the scalar product. Let us assume a square sample of side length L and set the boundaries as $\Gamma=\Gamma^L\cup\Gamma^R\cup\Gamma^B\cup\Gamma^T$, where

$$\Gamma^L=\{(x,z)\in\Gamma: x=0\},\quad \Gamma^R=\{(x,z)\in\Gamma: x=L\},$$

$$\Gamma^B=\{(x,z)\in\Gamma: z=0\},\quad \Gamma^T=\{(x,z)\in\Gamma: z=L\}.$$

[13] In other words, Γ^L, Γ^R, Γ^B, and Γ^T are the left, right, bottom, and top boundaries of the sample, respectively. Denote by $\boldsymbol{n}$ the unit outer normal on Γ and let $\boldsymbol{m}$ be a unit tangent on Γ so that $\{\boldsymbol{n},\boldsymbol{m}\}$ is an orthonormal system on Γ.

[14] To estimate the effective complex stiffnesses, we use a finite element procedure to approximate the solution of the equation of motion (20). We use bilinear functions to approximate the solid displacement vector, and we consider the solution of equation (20) with the following boundary conditions:

$$[\boldsymbol{\sigma}(\boldsymbol{u})\cdot\boldsymbol{n}]\cdot\boldsymbol{n}=-\Delta P,\quad (x,z)\in\Gamma^T, \tag{21}$$

$$[\boldsymbol{\sigma}(\boldsymbol{u})\cdot\boldsymbol{n}]\cdot\boldsymbol{m}=0,\quad (x,z)\in\Gamma^T, \tag{22}$$

$$[\boldsymbol{\sigma}(\boldsymbol{u})\cdot\boldsymbol{n}]\cdot\boldsymbol{m}=0,\quad (x,z)\in\Gamma^L\cup\Gamma^R, \tag{23}$$

$$\boldsymbol{u}\cdot\boldsymbol{n}=0,\quad (x,z)\in\Gamma^L\cup\Gamma^R, \tag{24}$$

$$\boldsymbol{u}=0,\quad (x,z)\in\Gamma^B. \tag{25}$$

[15] The medium is not allowed to move at the bottom and lateral boundaries $\Gamma^B\cup\Gamma^L\cup\Gamma^R$, a uniform time-harmonic compression of the form $\Delta P\exp(\mathrm{i}\omega t)$, where P denotes pressure, is applied at the top boundary Γ^T and no tangential external forces are applied. The factor $\exp(\mathrm{i}\omega t)$ is omitted because the problem is formulated in the space-frequency domain. A uniform compression can also be applied, for example, on a lateral boundary Γ^R, and in this case the boundary conditions (21), (24), and (25) become

$$[\boldsymbol{\sigma}(\boldsymbol{u})\cdot\boldsymbol{n}]\cdot\boldsymbol{n}=-\Delta P,\quad (x,z)\in\Gamma^T\cup\Gamma^R, \tag{26}$$

$$\boldsymbol{u}\cdot\boldsymbol{n}=0,\quad (x,z)\in\Gamma^L\cup\Gamma^B. \tag{27}$$

[16] Denoting by V the original volume of the sample, its (complex) oscillatory volume change, $\Delta V(\omega)$, allows us to define the *effective* P wave complex stiffness $p(\omega)$, by using the relation

$$\frac{\Delta V(\omega)}{V}=-\frac{\Delta P}{p(\omega)}. \tag{28}$$

[17] After solving equation (20) with the boundary conditions (21)–(25), the vertical displacements $u_3(x,z,L,\omega)$ on Γ^T allow us to obtain an average vertical displacement $u_3^T(\omega)$ at the boundary Γ^T. Then, for each frequency ω, the volume change produced by the compressibility test can be approximated by $\Delta V(\omega)\approx Lu_3^T(\omega)$, which enable us to compute $p(\omega)$ by using the relation (28).

[18] To obtain the *effective* shear stiffness, we consider the solution of equation (20) with the following boundary conditions:

$$-\boldsymbol{\sigma}(\boldsymbol{u})\cdot\boldsymbol{n}=g,\quad (x,z)\in\Gamma^T\cup\Gamma^L\cup\Gamma^R, \tag{29}$$

$$\boldsymbol{u}=0,\quad (x,z)\in\Gamma^B, \tag{30}$$

Table 1. Material Properties

Medium	λ (GPa)	μ (GPa)	ρ (kg/m^3)	c_P (m/s)	c_S (m/s)	Q_{01}	Q_{02}
Shale	6.28	1.70	2250	2074	869	60	20
Limestone	30	25	2700	5443	3043	80	40

where

$$g = \begin{cases} (\Delta p, 0), & (x,z) \in \Gamma^T, \\ (0, -\Delta p), & (x,z) \in \Gamma^L, \\ (0, \Delta p), & (x,z) \in \Gamma^R. \end{cases}$$

[19] *Santos et al.* [2009] show that uniqueness holds for equation (20) with the above boundary conditions for $\omega > 0$ sufficiently small, and that the associated error is of the order of the computational mesh size.

[20] The change in shape of the sample allows us to recover its equivalent complex shear stiffness $p(\omega)$ by using the relation

$$\tan[\theta(\omega)] = \frac{\Delta p}{p(\omega)}, \tag{31}$$

where $\theta(\omega)$ is the departure angle between the original positions of the lateral boundaries and those after applying the shear stresses [e.g., see *Kolsky*, 1963]. Equations (28) and (31) are valid in the quasi-static approximation. i.e., when the wavelength is much larger than the size of the sample. The horizontal displacements $u_1(x, L, \omega)$ at the top boundary Γ^T can then be used to obtain an average horizontal displacement $u_1^T(\omega)$ at the boundary Γ^T. Then, $\tan[\theta(\omega)] \approx u_1^T(\omega)/L$ and $p(\omega)$ can be calculated from equation (31).

[21] These experiments show how to obtain the stiffnesses associated with the symmetry axis and the layering direction, e.g., p_{33} and p_{11}, respectively, for the qP-wave, and p_{55} and p_{66} for the qSV and SH waves. Figures 1a–1e illustrate the five experiments we need to compute the stiffnesses components. The first two experiments use the boundary conditions (21)–(25). In (a) we obtain the stiffness p_{33}, while in (b) we obtain p_{11}. In this last case we rotate the boundary conditions (21)–(25) clockwise, by replacing Γ^T by Γ^R, Γ^R by Γ^B, Γ^B by Γ^L, and Γ^L by Γ^T. On the other hand, using the boundary conditions (29) and (30), we obtain the stiffness p_{55} by performing the experiment shown in (c) and the stiffness p_{66} with the experiment shown in (e). In this last case, the boundary conditions are the same as those used for p_{55} but replacing z by y in equations (20), (29), and (30).

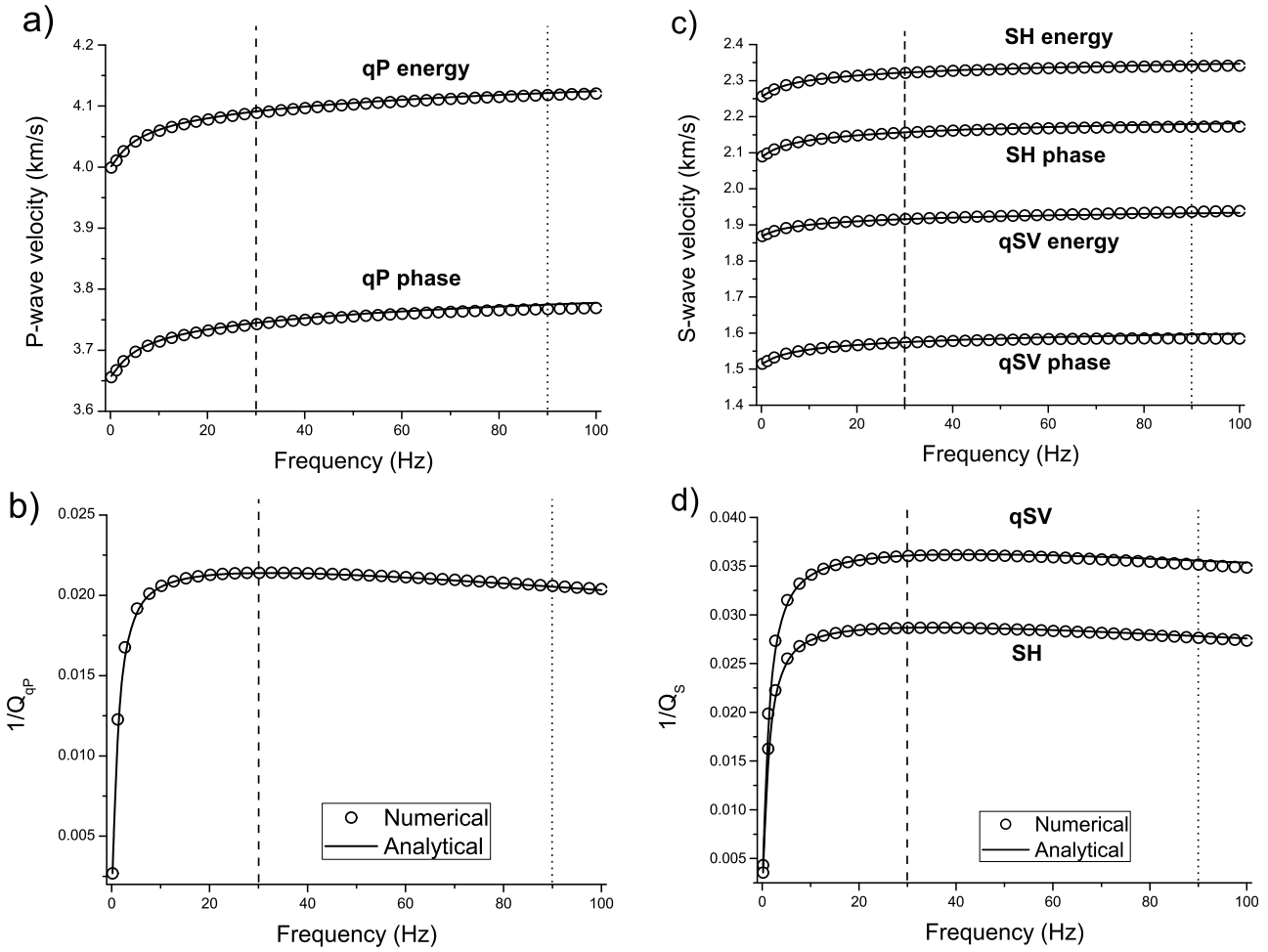

Figure 2. (a) qP-wave phase and energy velocities, (b) qP-wave quality factor, (c) S-wave phase and energy velocities and (d) S-wave quality factor as a function of frequency obtained with the oscillatory tests (symbols) and Backus theory (solid line). The propagation angle is $\theta = 60°$. We observe an excellent agreement until about 90 Hz (vertical dotted line).

[22] Finally, to compute p_{13} we apply a normal stress $\sigma = \sigma_{11} = \sigma_{33}$ as shown in Figure 1d. The stress-strain relations for a transversely isotropic medium are

$$\begin{aligned} \sigma_{11} &= p_{11}\epsilon_{11} + p_{13}\epsilon_{33}, \\ \sigma_{33} &= p_{13}\epsilon_{11} + p_{33}\epsilon_{33}, \end{aligned} \tag{32}$$

[*Carcione*, 2007, equation (4.4)], where ϵ_{33} and ϵ_{11} are the strain components at the top side and at the right lateral side of the sample, respectively. Using the boundary conditions (22), with Γ^T replaced by $\Gamma^T \cup \Gamma^B$, (23), (26), and (27), we compute the displacements and obtain p_{13} from equations (32) as

$$p_{13} = \frac{p_{11}\epsilon_{11} - p_{33}\epsilon_{33}}{\epsilon_{11} - \epsilon_{33}}. \tag{33}$$

4. Example

[23] The example considers the shale-limestone periodic layered medium described by *Carcione* [1992]. The properties of the isotropic viscoelastic materials are given in Table 1, i.e., the low-frequency Lamé constants, wave velocities, densities and quality factors. Let the time constants in equation (5) be $\tau_1 = 0.16$ s and $\tau_2 = 0.3$ ms, so that the quality factor of each single isotropic layer is nearly constant over the exploration seismic band (from about 10 Hz to 100 Hz). In the long-wavelength limit, the wave characteristics of the layered medium are defined by the Backus averaging relations (4), the phase velocities (8), the energy velocities (9) and (13), and the quality factors (16). In order to validate Backus theory we perform the numerical compressibility and shear oscillatory tests described in section 3. The stratified medium is a 50 cm side sample composed of 100 alternating plane layers of shale and limestone of equal thickness. The spatial period of the layering is then 1 cm. The finite element simulations uses a uniform mesh of 100 × 100 elements.

[24] Figure 2 displays the modulus of the phase and energy velocity vectors (Figures 2a and 2c) and quality factor (Figures 2b and 2d) as a function of frequency, obtained with the oscillatory tests (symbols), compared to Backus theory generalized to the lossy case by *Carcione* [1992] (solid line). The propagation angle corresponding to the phase velocity is $\theta = 60°$. The corresponding energy angles are $\psi = 83.7°$ for the qP wave, $\psi = 25.3°$ for the qSV wave and $\psi = 81.8°$ for the SH wave. It is seen that anisotropy implies quite different phase and energy velocity curves. We observe an excellent agreement between the theoretical and numerical results until about 90 Hz (vertical dotted line).

[25] Figure 3 shows polar representations of the phase velocity vector (Figure 3a), energy velocity vector (Figure 3b) and quality factor (Figure 3c) at 30 Hz. The polar curve for the quality factor is given by $(\sin\psi, \cos\psi)\, Q$. Both the phase and energy angles are indicated. As before, the agreement is excellent. Moreover, this plot shows that attenuation anisotropy due to fine-layering is more pronounced for shear waves than for compressional waves. In this case, the qP-, qSV- and SH-wave wavelengths along the symmetry axis ($\theta = 0$) are 92 and 42 m, respectively. Therefore the dominant wavelength (at 30 Hz) to spatial period ratio is 9200 and 4200, respectively, i.e., well within the long-wavelength limit (which,

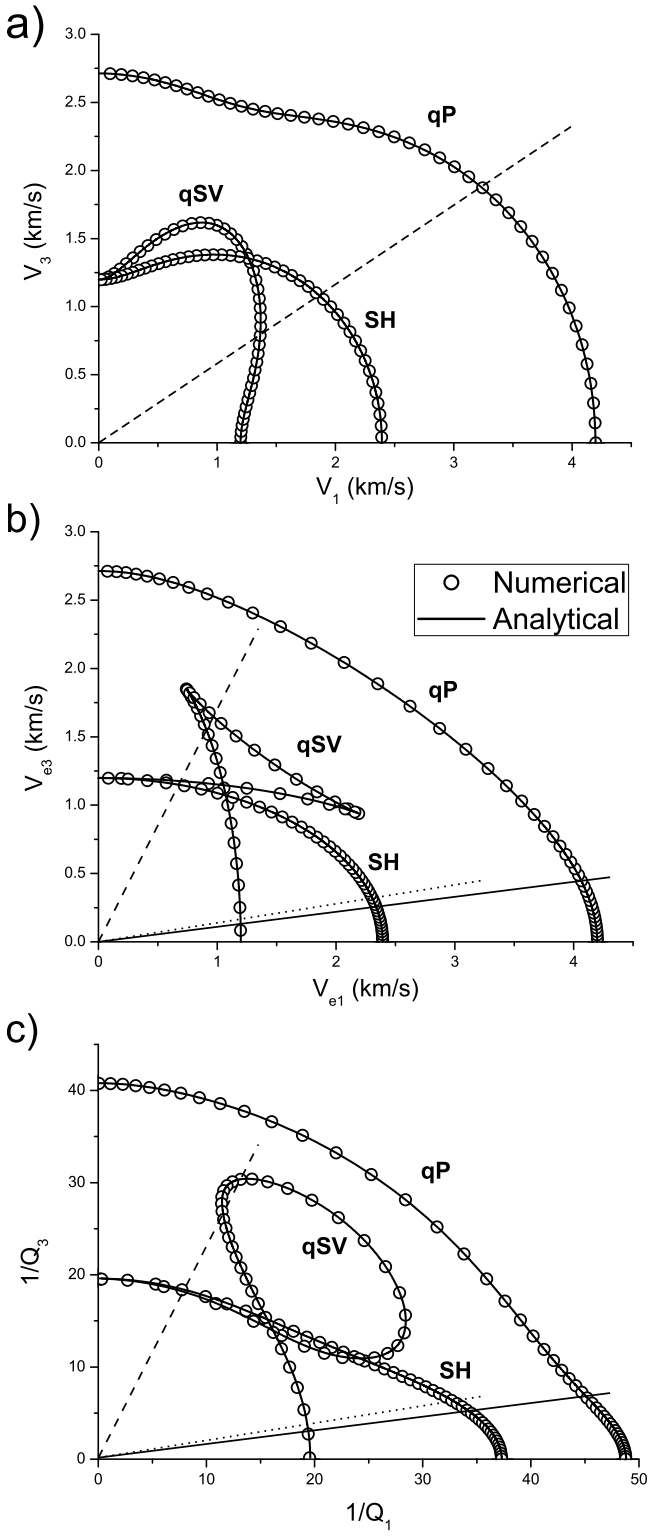

Figure 3. Polar representation of the (a) phase velocity vector, (b) energy velocity vector and (c) quality factor corresponding to a frequency of 30 Hz (the vertical dashed lines indicated in Figure 2). The symbols represent the numerical simulations. The dashed line in Figure 3a corresponds to the phase angle $\theta = 60°$. The solid, dashed and dotted lines in Figures 3b and 3c correspond to the energy angles $\psi = 83.7°$ (qP wave), $\psi = 25.3°$ (qSV wave) and $\psi = 81.8°$ (SH wave).

in theory, is between 5 and 8 for P waves approximately, and depending on the single constituents).

5. Conclusions

[26] The Backus/Carcione theory describes the anisotropic behavior of finely-layered media at long wavelengths. Here, we have introduced a novel numerical method based on oscillatory experiments to test the theory, i.e., we obtain the complex and frequency-dependent stiffnesses which allow us to compute the wave velocities and quality factors as a function of frequency and propagation angle. The methodology is based on a finite element solution of the equations of motion in the space-frequency domain to simulate harmonic compressibility and shear tests. We consider a periodic sequence of shale and limestone. The agreement between the numerical and theoretical results is excellent. The method validates the anelastic theory for Q-anisotropy and, in addition, the expressions of the wave velocities and Q factors for homogeneous viscoelastic body waves in anisotropic media.

[27] Laboratory measurements indicate that attenuation is related to the presence of fluids. In particular, attenuation may be used as an indicator of permeability and fluid saturation. Attenuation anisotropy is more pronounced than velocity anisotropy. Hence, measurements of Q-anisotropy may provide more reliable information about the orientation of layering and fractures, and fluid properties of hydrocarbon reservoirs. Shear wave experiments can provide useful information, since it is seen that attenuation anisotropy due to fine-layering is more pronounced for shear waves than for compressional waves.

[28] The theory and numerical solver proposed in this work can be applied to more complex geological situations (lower symmetries, stochastic heterogeneities, fractures, etc.) and implemented in the processing and interpretation of real seismic data for characterization purposes.

References

Auld, B. A. (1990), *Acoustic Fields and Waves in Solids*, vol. 1, Krieger, Malabar, Fla.

Backus, G. E. (1962), Long-wave elastic anisotropy produced by horizontal layering, *J. Geophys. Res.*, *67*, 4427–4440.

Ben-Menahem, A. B., and S. J. Singh (1981), *Seismic Waves and Sources*, Springer, New York.

Bruggeman, D. A. G. (1937), Berechnungen der verschiedener physikalischen Konstanten von heterogenen Substanzen. III: Die elastischen Konstanten der quasi-isotropen Mischkörper aus isotropen Substanzen, *Ann. Phys.*, *29*, 160–178.

Carcione, J. M. (1992), Anisotropic Q and velocity dispersion of finely layered media, *Geophys. Prospect.*, *40*, 761–783.

Carcione, J. M. (2007), *Wave Fields in Real Media: Wave Propagation in Anisotropic, Anelastic, Porous and Electromagnetic Media*, *Handb. Geophys. Explor.*, vol. 38, 2nd ed., Elsevier, Boston.

Carcione, J. M., and F. Cavallini (1994), A rheological model for anelastic anisotropic media with applications to seismic wave propagation, *Geophys. J. Int.*, *119*, 338–348.

Carcione, J. M., and F. Cavallini (1995), Attenuation and quality factor surfaces in anisotropic-viscoelastic media, *Mech. Mat.*, *19*, 311–327.

Carcione, J. M., D. Kosloff, and A. Behle (1991), Long wave anisotropy in stratified media: A numerical test, *Geophysics*, *56*, 245–254.

Carcione, J. M., F. Cavallini, and K. Helbig (1998a), Anisotropic attenuation and material symmetry, *Acustica*, *84*, 495–502.

Carcione, J. M., H. Helle, and T. Zhao (1998b), The effects of attenuation and anisotropy on reflection amplitude versus offset, *Geophysics*, *63*, 1652–1658.

Kolsky, H. (1963), *Stress waves in solids*, Dover, New York.

Liu, H. P., D. L. Anderson, and H. Kanamori (1976), Velocity dispersion due to anelasticity; implications for seismology and mantle composition, *Geophys. J. R. Astron. Soc.*, *47*, 41–58.

Postma, G. W. (1955), Wave propagation in a stratified medium, *Geophysics*, *20*, 780–806.

Riznichenko, Y. V. (1949), Seismic quasi-anisotropy, *Bull. Acad. Sci. USSR, Geograph. Geophys. Serv.*, *13*, 518–544.

Santos, J. E., J. G. Rubino, and C. L. Ravazzoli (2009), A numerical upscaling procedure to estimate effective plane wave and shear moduli in heterogeneous fluid-saturated poroelastic media, *Comput. Methods Appl. Mech. Eng.*, *198*, 2067–2077.

Schoenberg, M., and F. Muir (1989), A calculus for finely layered media, *Geophysics*, *54*, 581–589.

Sidler, R., J. M. Carcione, and K. Holliger (2008), On the evaluation of the plane-wave reflection coefficients in anelastic media, *Geophys. J. Int.*, *175*, 94–102.

J. M. Carcione, D. Gei, and S. Picotti, Istituto Nazionale di Oceanografia e di Geofisica Sperimentale, OGS, Borgo Grotta Gigante 42/c, I-34010 Sgonico, Italy. (spicotti@inogs.it)

J. E. Santos, CONICET, Departamento de Geofísica Aplicada, Facultad Ciencias Astronómicas y Geofísicas, UNLP, Paseo del Bosque S/N, La Plata 1900, Argentina.